Research Square

Preprints are preliminary reports that have not undergone peer review.
They should not be considered conclusive, used to inform clinical practice,
or referenced by the media as validated information.

Direct-from-Wood Fibrillation for Self-Binding Porous Materials: a novel valorization pathway for residual wood and coarse wool waste

Jemma Eloise Gillon
Swiss Federal Laboratories for Materials Science and Technology
Thomas Geiger
thomas.geiger@empa.ch

Swiss Federal Laboratories for Materials Science and Technology

Research Article

Keywords:

Posted Date: November 25th, 2026

DOI: https://doi.org/10.21203/rs.3.rs-11478173/v1

License: This work is licensed under a Creative Commons Attribution 4.0 International License.
Read Full License

Additional Declarations: No competing interests reported.

Noname manuscript No.
(will be inserted by the editor)

Direct-from-Wood Fibrillation for Self-Binding Porous Materials: a novel valorization pathway for residual wood and coarse wool waste

Jemma E. Gillon · Thomas Geiger

Received: date / Accepted: date

Abstract Identifying viable valorization pathways for biogenic waste streams has become increasingly important in the context of the climate crisis. In this work, forestry waste, in combination with industrial waste wool, was processed through simple and direct methods in order to achieve a foam-like material. Different energy inputs were explored for direct-from-source fibrillation. 5 kWh/kg_{wood} resulted in a multiscale mix of wood particles and fibrils, here defined as wood fibrils, providing the porous material with sufficient stability and preventing significant shrinkage during drying. When incorporating industrial waste wool, samples with λ-values as low as 64 $mW/(m \cdot K)$ were achieved. Additionally, the incorporation of waste wool increased hygroscopic and fire-retardant properties. Wood fibrils were combined with guanidine phosphate and aluminum hydroxide (20 wt%). Guanidine phosphate enabled self-extinguishing behavior, while both routes showed improved thermal degradation management, supporting development towards practical applications. This work demonstrates that the inherent binding properties of low-energy fibrillated residual wood enable the development of bio-based, porous material systems. The mechanical, thermal and fire-performance of these systems can be tailored by incorporating different components, such as organic and inorganic flame-retardants, as well as industrial waste wool, creating new opportunities for waste valorization.

Keywords Residual wood · Waste wool · Wood fibrils · Waste wood · Bio-based binder

J. E. Gillon
Cellulose and Wood Materials Laboratory, Empa – Swiss Federal Laboratories for Materials Science and Technology, Dübendorf, Switzerland
E-mail: jemma.gillon@empa.ch
0009-0007-3517-5029

T. Geiger (*)
Cellulose and Wood Materials Laboratory, Empa – Swiss Federal Laboratories for Materials Science and Technology, Dübendorf, Switzerland
E-mail: thomas.geiger@empa.ch
0000-0001-6555-8417

1 Introduction

Industrial biomass generates waste globally, to an extraordinary degree. Total global wood residues were estimated to amount to 226 million metric tons in 2025 (Weldesemayat Sileshi et al., 2025). This number, however, excludes primary waste generated by forestry, which was estimated at an even greater 960 Mt (van den Born et al., 2014). In a functioning circular economy model, this would constitute a large material reservoir (EEA, 2026). But without viable valorization pathways and the corresponding infrastructure, this mainly results in a waste disposal problem. The primary use of residual wood is in energy recovery (Malinverno et al., 2024), losing wood's value not only as a carbon sink, but also destroying the hierarchical fiber architecture of the cell wall in the process. This consists of oriented cellulose fibrils at the nanometer scale that provide strength, stiffness, and porosity and difficult to be reproduced synthetically.

According to the Finnish Sawmillmen Association, one unbarked saw log results in 45–50 % sawn timber, 28–32 % wood chips, 10–15 % sawdust and 10–12 % bark (Sahateollisuuskirja, 2026). Of these by-products, wood chips are the most valuable, and used mainly for pulp and paper production. Sawdust can be used in energy generation, panel manufacturing, and pulp production. In regions without a panel industry, sawdust is burned in open fires or landfilled. In one documented case, 60 %

of the total volume generated remained unused (Adu et al., 2014). Bark differs fundamentally from wood in its chemical composition. It contains higher levels of extractives, polyphenols, and tannins, as well as a different type of lignin, which alters the fibrillation behavior and property profile of the resulting material compared to pure wood (Sjöström, 1993). Aside from some uses in landscaping and gardening, bark is mainly used for energy generation (Kunttu et al., 2020).

When approaching the issue of industrial waste valorization, yield is incredibly important for economic consideration. The established method of producing cellulose nanofibrils (CNF), via complete disintegration, is unsuitable for this approach, as it incurs low yields, large chemical input, and high energy costs (Solala et al., 2020). Lignocellulosic nanofibrils (LCNF) achieve comparatively higher yields. In one study, a yield of 85 % was attained for LCNF derived from poplar wood chips, via a Kraft-pulping route (Zhang et al., 2022). Direct fibrillation without chemical or biological pretreatment steps has been demonstrated. Yousefi et al. (2018) isolated wood nanofibrils measuring 55 ± 22 nm purely mechanically and without the use of chemicals. It has been shown that energy inputs of 10-13 kWh/kg (Dudnyk et al., 2025; Tarrés et al., 2020) lead to LCNF, which as raw material can be used in the further production of films, boards and gels. LCNF made from undelignified sawdust achieves tensile film strengths of 100 MPa at the same energy level as bleached kraft pulp (Ämmälä et al., 2021).

355'000 Swiss sheep (BFS, 2026) produce around 900 metric tons of raw wool annually (LID, 2025). These sheep are mainly dairy and meat sheep, and produce coarser wool, undesirable for garments. While each sheep costs approximately CHF 6 to shear, the resulting revenue is generally less than CHF 2 per sheep (SRF, 2022). The European price of wool is even lower, at less than 0.30 Euros per kilogram (Mad'in, 2025). When there are no routes available for wool valorization, the wool must be disposed of at a cost (SRF, 2025). In Switzerland, roughly one-fifth is burnt (SRF, 2019). In the United Kingdom, the garment industry alone was estimated to produce 164'984 tons of wool waste (Thomas et al., 2012). Wool waste is thus a pressing issue, and the disposal thereof leads to burdensome costs, release of CO2, and, in some cases, local environmental pollution (Camilli et al., 2025).

The wool material used in this work is noil, which is separated as the short-fiber fraction during the combing stage of yarn production (Lawrence, 2003). It is washed, degreased, and cleaned, in a process that preserves the fiber structure, because the separation is purely mechanical. In this study, the noil is further reduced in length by mechanical milling and mixed directly with the fibrillated wood residue. Previous studies have shown that fibrils derived from sawmill residues have diameters ranging from 5 to 55 nm and lengths from 100 to 900 nm (Miao et al., 2024; Yousefi et al., 2018), meaning they differ by roughly 3 orders of magnitude in size to the wool used in this work.

In comparison to the cited literature, this study used unscreened mixed species forestry waste as the feedstock. Previous studies have worked within single species frameworks. We aim to show that waste wood across a broad range can be utilized for valorization into a self-binding, porous material, without the need for chemical pretreatment or fractionation. Direct fibrillation of this material does not produce a homogeneous nanomaterial, but rather a broad spectrum of particles and LCNF in the nanometer to micrometer range, containing both wood and bark components. As this is a heterogeneous material, it has been termed wood fibrils (WF) to distinguish from LCNF alone. The specific fibrillation energies (SFE) of 5 and 10 kWh/kg used in this study are at the lower end of the range reported in the literature. This range was specifically chosen to evaluate the most energy-efficient processing option and to compare its material quality with that achieved at higher energy levels. The resulting WF is used as a biogenic binder and mixed with wool noil. Subsequent oven drying produces a foam-like material, whose mixing and structural properties are systematically investigated. To validate the material for real-world application scenarios, WF are additionally combined with two flame retardants: aluminum hydroxide (ATH) and guanidine phosphate (GP). The thermal, mechanical, and hygroscopic properties are characterized, and potential areas of application are discussed.

2 Experimental

2.1 Materials

Wood chips consisting of residual wood from forestry, including bark, from an unspecified mix of hard- and softwood were collected from the Holzkorporation Dübendorf (Dübendorf, Switzerland). No further sorting or cleaning was performed prior to processing. Waste wool in the form of noil (4 kg) was provided by Baur Vliesstoffe GmbH (Germany)/Swisswool (Switzerland). For comparison with fibrillated wood, additional samples were prepared using a commercial CNF suspension (Valida S231C, 8 wt%, Sappi Maastricht BV, Netherlands). To explore functional tuning pathways, two flame-retardant systems were incorporated: guanidine phosphate (GP; CAS No: 5423-23-4, TCI, Japan) and

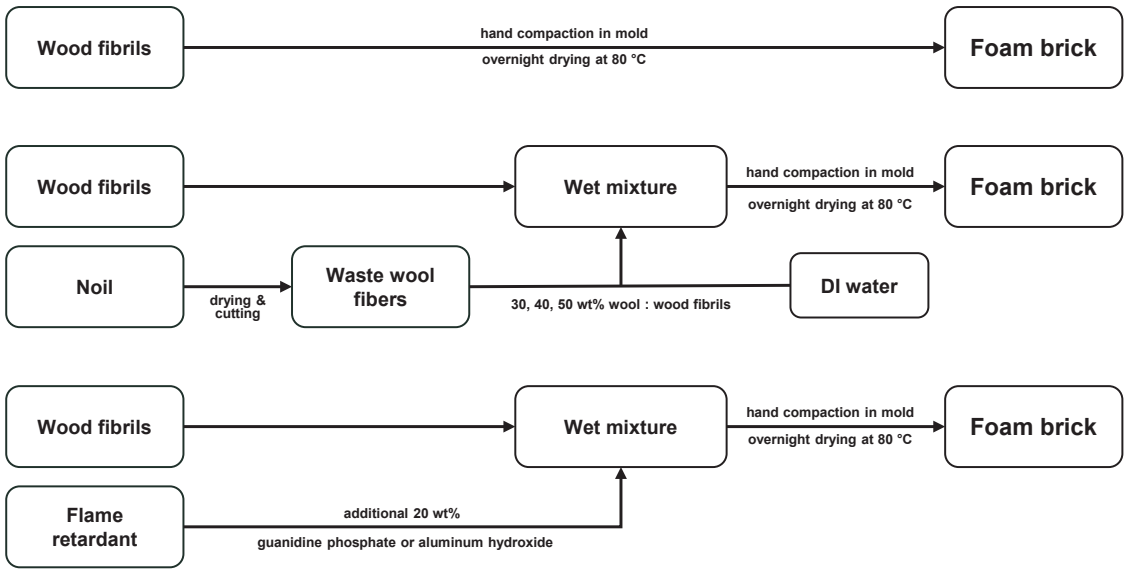


Fig. 1 Schematic of the sample production process, showing the three different types of porous materials made. Wood fibrils were used directly, or mixed with wool or flame retardants. After molding and drying overnight, the resulting material was lightweight and foam-like.

aluminum hydroxide (ATH; CAS No: 21645-51-2, Sigma-Aldrich, USA)

2.2 Material Preparation

Wood chips were dried in a convection oven (450 UF plus, Memmert GmbH + Co. KG, Germany) at 105 °C for 12 h. The dried chips were cut using a cutting mill (SM 2000, Retsch GmbH, Germany), equipped with a 4 mm sieve insert, to produce wood fibers in one pass with no additional particle size screening. A wood fiber slurry was first soaked overnight and then adjusted to 6.6 wt% with deionised (DI) water. This was then passed repeatedly through a super masscolloider (MKZA10-20J CE, Masuko Sangyu Co., Ltd, Japan) operating at 1450 rpm until an SFE of 5 kWh/kg_{wood} was achieved, named 5WF. This process is schematically presented in the top row in Fig. 1. After fibrillation, the slurry was dewatered in textile bags under 200 kg overnight. To determine the solids content, five approximately 5 g samples were dried at 105 °C to constant mass. The solids content of the resulting dispersion was found to be 19 wt%. A further batch was made with an SFE of 10 kWh/kg_{wood}, analogously named 10WF. Dewatering required an additional 5 h and the solids content was determined as 19.8 wt%. Prior to processing, the waste wool was dried overnight at 105 °C in a convection oven and subsequently passed through the cutting mill with a 4 mm sieve insert.

2.3 Sample Preparation

The sample preparation is schematically shown in the lower part of Fig. 1. All formulations were produced as aqueous dispersions containing a total solids content of 19 wt% and DI water, prior to drying. Mixtures were prepared with 0, 30, 40 and 50 wt% waste wool fibers (dry mass basis) and 5WF. Mechanical mixing was performed using a kitchen mixer (Cooking Chef XL KCL95.004SI, Kenwood, UK) equipped with the K-hook attachment. The mixture was processed for 5 min at the manufacturer's lowest speed setting. To investigate the influence of higher specific fibrillation energy input, additional samples were prepared using 10WF following the same procedure, with 0 wt% and 50 wt% waste wool fibers. Two flame retardant systems were investigated. GP and ATH were added at 20 wt% relative to the dry mass of 5WF. After mixing, the resulting masses were compacted by hand into a 5-sided plastic mold with inner dimensions of 41 mm × 84 mm × 101 mm. The molded specimens were removed, weighed in the wet state and dried in a convection oven (UF 110 plus, Memmert GmbH + Co. KG, Germany) at 80 °C overnight. After removal from the oven, the dry weight was recorded for the determination of the solids content. CNF samples containing 0 and 50 wt% waste wool fibers were made by the same process of mixing for 5 min, molding, and drying at 80 °C, although the target solids content was kept at 8 wt% due to dewatering difficulties. One

additional sample was made using 5WF with a target solids content of 8 wt% for shrinkage comparison. The name of each sample contains the SFE of the fibrillated wood and the solids content of each component, e.g. 5WF50W50 is a sample made using 50 wt% 5WF and 50 wt% waste wool fibers.

2.4 Microscopy

Scanning electron microscopy (SEM; FEI Quanta 650 FEG ESEM) was used to investigate the morphology of the different fibrillated wood batches. A droplet of 0.05 wt% suspension was placed on mica. Additional samples were prepared from molded and dried blocks in order to explore the final morphology. All samples and dispersions were sputter-coated with 7 nm platinum (MED 020, Bal-tec) and imaged at an operating voltage of 5 kV. Additional imaging on the molded and dried blocks was conducted with a stereoscope (Stemi SV 11, Zeiss, Germany). Evaluation of the fibril diameter D and the pore size was conducted with imaging software ImageJ (National Institutes of Health, USA), using the line measurement tool.

2.5 Density

The apparent density ρ (kg/m^3) was characterized using samples cut to size from one main block using a band saw. The dimensions were 15 mm × 15 mm × 25 mm, and the samples were first conditioned in 50 % relative humidity (RH) at 23 °C. For each sample, the height, width, and length were measured at three positions using a digital caliper, and the average values were used to calculate the specimen volume. The specimens were weighed using an analytical balance, and the density was calculated as the ratio of mass to measured volume. Five specimens were analyzed from one representative block per formulation.

2.6 Shrinkage

Volumetric shrinkage (%) was determined from three blocks per formulation. The initial wet volume (V_{wet}) corresponded to the mold dimensions. After drying, the block dimensions were measured and the final dry volume (V_{dry}) calculated. Volumetric shrinkage was determined as:

$$Shrinkage(\%) = \frac{V_{wet} - V_{dry}}{V_{wet}} \times 100 \quad (1)$$

2.7 Thermogravimetric analysis

Thermogravimetric analysis (TGA; TG 309 Libra, Netzsch, Germany) was conducted in an atmosphere of air from 30–800 °C, with a heating rate of 10 K/min. The measurements were analyzed using the corresponding instrument software (Proteus, Netzsch, Germany), in which automatic analysis in combination with derivative (DTG) curves were used to identify distinct mass loss stages. Samples were first dried at 105 °C and stored in a desiccator chamber containing a drying agent before testing.

2.8 Thermal Conductivity

Thermal conductivity λ (mW/(m · K)) was tested using a guarded hot plate device based on EN 12667. The device consisted of a lower cooling plate and an upper guarded hot plate at the top, between which the specimen is positioned. The apparatus has an accuracy of ±10 % when comparing different material types (Canto et al., 2023). From each block, two flat interior horizontal slices were cut, using a band saw. The thickness of each specimen was measured prior to testing and ranged between 8–13 mm. All slices were conditioned in 50 % RH at 23 °C for at least 24 h before testing. Measurements were conducted in a climate chamber maintained in 50 % RH at 23 °C.

2.9 Uniaxial Compression

Uniaxial compression tests were conducted using a universal testing machine (Z005 AllroundLine, ZwickRoell GmbH + Co. KG, Germany) equipped with a 5 kN load cell. Specimens (15 mm × 15 mm × 25 mm) were cut to size via band saw. In order to explore anisotropy within the sample, two sample types were cut. The first were cut along the horizontal axis, the second along the vertical axis. They were conditioned in 50 % RH at 23 °C for at least 24 h prior to testing. Compression tests were performed with a pre-load of 0.5 N and a crosshead speed of 5 mm/min. The test was terminated at either 2000 N or a 5 mm head distance, whichever occurred first. Young's modulus E (MPa) was determined from the linear elastic region of the stress-strain curve immediately after the onset.

2.10 Moisture Uptake

The same samples initially used for thermal conductivity characterization were dried at 105 °C for 24 h until

constant mass was reached. The oven-dry mass was recorded as m_{dry}. The specimens were then transferred sequentially into chambers with the following RH and temperature conditions: 35 % at 20 °C, 50 % at 23 °C, 65 % at 20 °C, 85 % at 20 °C, and finally returned to 35 % at 20 °C. Each transfer occurred after equilibrium moisture content was reached, defined as a mass change of less than 0.1 wt% over 24 h.

Moisture uptake (MU) was calculated as:

$$MU(\%) = \frac{m - m_{dry}}{m_{dry}} \times 100 \quad (2)$$

2.11 Preliminary Flammability Testing

Each formulation made using 5WF, waste wool fibers, GP and ATH, was evaluated in a preliminary, laboratory scale setup for flammability behavior. The blocks were cut with a band saw lengthwise into columnar specimens with cross-sectional dimensions of 15 mm × 15 mm and a length of 80–90 mm. All specimens were conditioned in 50 % RH at 23 °C for at least 24 h prior to testing. Of each composition, 3 columnar specimens were tested. Specimens were clamped horizontally, and a Bunsen burner with a luminous flame was positioned at an angle of 45° relative to the sample axis, where it was in contact for 15 s. The samples were allowed to burn freely for 2 min, while being monitored with an infrared camera (testo 880, Testo SE & Co. KGaA, Germany; max T = 355 °C) and video recordings. Single frames were captured with the infrared camera and evaluated for surface temperature. The procedure was analogous to the UL94 horizontal single-flame test, and designed to enable preliminary evaluation of relative flammability behavior between sample formulations.

3 Results and Discussion

3.1 Disintegration of wood fibers and formation of wood fibril networks

After implementing an SFE of 5 kWh/kg$_{wood}$ and dewatering under static load overnight, a solids dispersion of 19 wt% was achieved (Fig. 2a). This contained a mix of wood particles that were not fully broken down during fibrillation (Fig. 2b), as well as a distinct fraction of WF (Fig. 2c). Initial measurements of the 5WF SEM images indicated an average fibril diameter, D, of (109 ± 45) nm ($n = 56$), with a D_{min} of 36 nm. Previous studies on CNF morphology have shown that SEM imaging is capable of resolving larger fibrils ($D > 100$ nm), while TEM is more suitable for nanofibrils in the order of tens of nanometers or lower (Wang et al., 2012).

For a higher SFE input of 10 kWh/kg$_{wood}$, samples were taken at different stages of the process (Fig. 3a-i). It was possible to observe the development of the WF network. While residual wood particles remained even up to an SFE of 10 kWh/kg$_{wood}$ (Fig. 3f), comprehensive WF networks developed as early as 3 kWh/kg$_{wood}$ (Fig. 3b). Small WF fractions were even visible in the first sample at 1 kWh/kg$_{wood}$ (Fig. 3g). When comparing processing benchmarks, 10WF required an additional 5 h dewatering time to achieve a similar solids content of 19.8 wt%. This indicates an increased degree of fibrillation (DOF), as the larger surface area of WFs likely interacted more with the surrounding water, slowing the release during dewatering. The measured fibril diameter D went from (110 ± 35) nm ($n = 35$, $D_{min} = 18$ nm), at 1 kWh/kg$_{wood}$, to (87 ± 38) nm ($n = 55$, $D_{min} = 25$ nm), at 10 kWh/kg$_{wood}$. These measurements were, however, done by hand using an imaging software, and more quantitative measurement techniques such as viscosity or turbidity could provide a more accurate picture of the DOF development.

In both SFE scenarios, a distinct WF fraction was achieved by using wood fibers from waste wood directly in a disk grinder, without the need for biological or chemical pretreatment to enable fibrillation.

3.2 Sample morphology

The samples were dried in a convection oven at 80 °C overnight. In Fig. 4, an example of each formulation is pictured, with 5WF60W40 chosen as representative of all wool containing blocks. Each sample had a distinctly different surface color than that of the bulk. When comparing Fig. 4a/b to Fig. 4e/f, the bulk is lighter than the surface. This is attributed to the migration of water-soluble components, such as hemicelluloses and extractives, towards the sample surface during drying, where they accumulate as water evaporates. Samples produced using 10WF exhibited a lighter surface coloration (Fig. 4c/d), suggesting that a greater fraction of these soluble components was first removed during the more intensive fibrillation process, which involved prolonged exposure to water. A white powdery layer was observed on the surface of 5WF100GP20 samples (Fig. 4h), resulting from the migration of dissolved GP to the surface during drying, followed by crystallization upon water evaporation. In contrast, no comparable surface layer was observed for 5WF100ATH20 (Fig. 4g), as ATH is insoluble in water and therefore did not migrate with the drying water. CNF100 had a yellowed surface (Fig. 4k) typical of dried solid CNF materials. CNF50W50 also displayed some unevenness of color associated with the wool content (Fig. 4l).

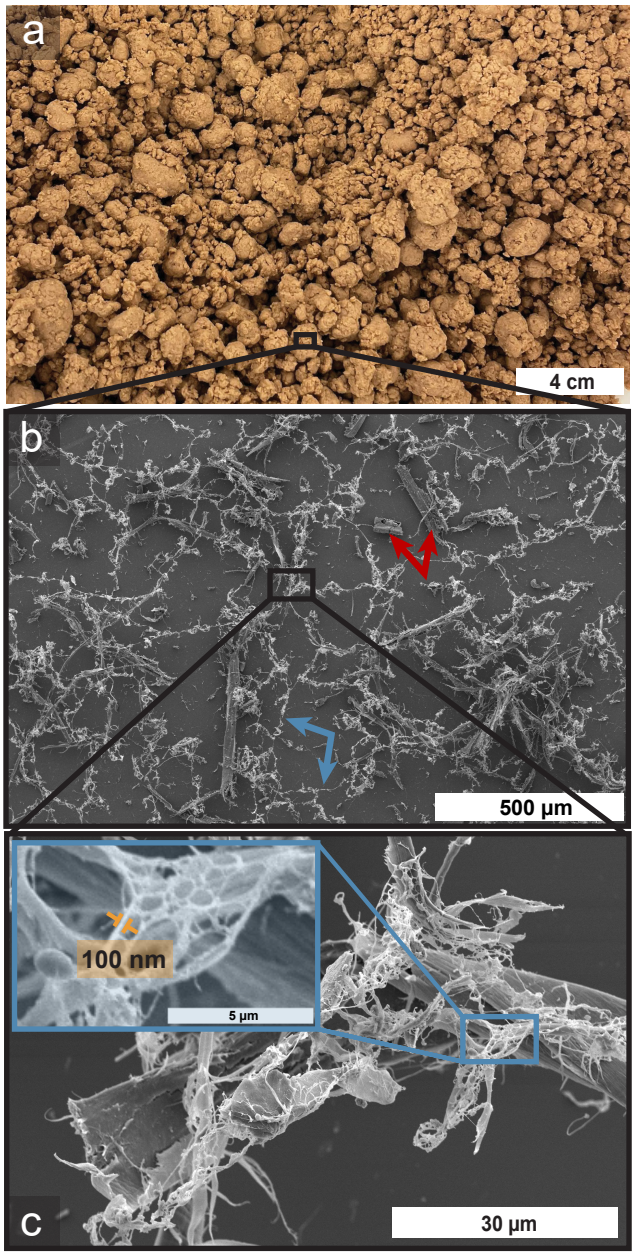


Fig. 2 Morphology of 5WF: (a) After fibrillation, dewatering under static load overnight results in a 19 wt% dispersion (b) Red arrows indicate remaining wood fibers and particles, blue arrows indicate WF networks (c) The WF wrap around wood particles, creating a network containing components across multiple scales.

Due to the simple mixing method, a small number of waste wool fiber clumps remained in the dispersion (Fig. 4f). The internal structure of 5WF100 is shown at the macroscopic and microscopic scales in Fig. 4e and 4i, respectively. This was found to be porous along the micro- and macroscale. Initial measurements from SEM pictures indicate that the micropores are in the range of tens of micrometers ($\varnothing_{PoreSize} = (19 \pm 17)$ µm, $n = 36$). The macropores are visible in Fig. 4e. Previous studies have implemented various foaming and freeze-drying methods to achieve lightweight, porous materials from CNF (Antonini et al., 2019; Wemmer et al., 2019; Josset et al., 2017). This resulted in well-defined pores, arising from stabilized air bubbles formed during the foaming process and ice-crystal formation. These methods produced extremely light-weight materials. In this work, no foaming step was implemented to increase the porosity. Thus the resulting materials are more dense than previously reported CNF foams and the pores are less well-defined.

Samples made entirely out of fibrillated wood often exhibited drying-induced stress-cracking. In this case, 5WF100 proved more stable than 10WF100. In the latter case, all samples contained cracks, and were thus not tested for mechanical or thermal properties. Given the increase in shrinkage values of 39.9 % to 56.2 % for 5WF100 and 10WF100 respectively (Tab. 1), a lower WF fraction was found to be advantageous in providing structural stability during drying. The presence of larger wood particles prevented the WF networks from collapsing and forming cracks during drying.

Analogous to this observation, when using CNF as a composite component, significant shrinkage was observed. For CNF100, made using the same processing steps, shrinkage reached 89.7 % (Fig. 4k), while the incorporation of wool reduced it slightly to 78.7 % (Fig. 4l). One test sample was made using 5WF with a target solids content of 8 wt% to get a more direct comparison. This had a measured shrinkage of 73 %. As the WF fibrillation process was entirely mechanical, the cell wall was disintegrated without any further chemical treatment. In classic CNF production, this additional chemical or biological processing results in freely accessible OH groups, which increase the hydrophilicity of the material. In contrast, the produced WF still had lignin and hemicelluloses interacting with the cellulose molecules, and thus likely exhibited greater hydrophobic properties. This resulted in more efficient water evaporation during drying through reduced capillary stresses, hindering collapse and shrinkage.

With the addition of a wool fraction, there was no occurrence of internal cracking. In fact, shrinkage was reduced to between 19.2–27.6 %. Thus the additional wool fibers functioned as a stabilizing component throughout the drying process. However, as can be seen in Fig. 4j, the wool fibers are only loosely embedded in the WF matrix, and there is limited mechanical interaction between the components.

These findings highlight that the multiscale structure consisting of WFs and wood particles provides structural stability during drying. In contrast, homogeneous CNF

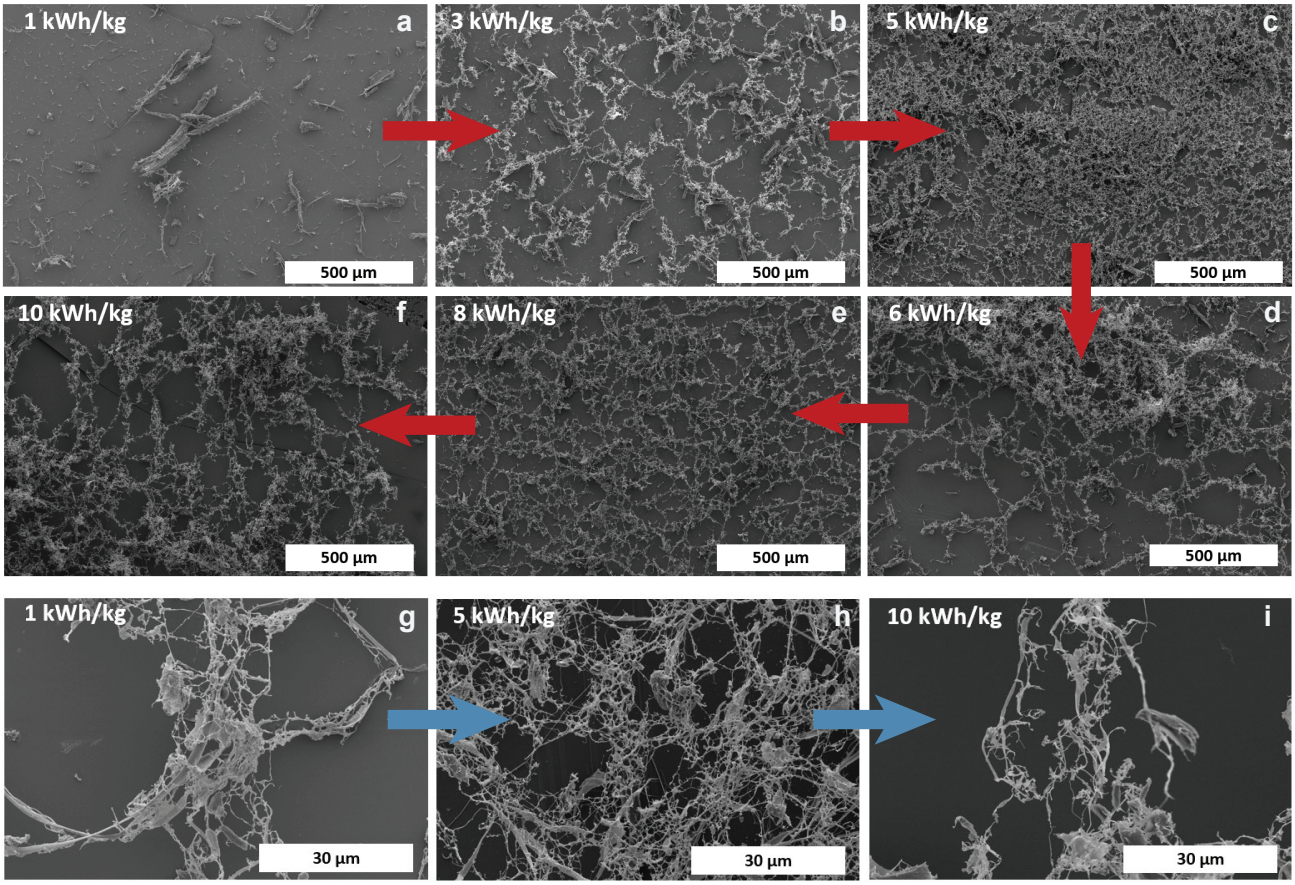


Fig. 3 (a)-(f): The red arrows show the progression throughout the fibrillation process up to 10 kWh/kg$_{wood}$. Comprehensive WF networks develop early, already forming at 3 kWh/kg$_{wood}$. (g)-(i): Up close, WF can already be observed at the lowest SFE (1 kWh/kg$_{wood}$)

Table 1 Overview of sample properties

Sample	ρ [kg/m^3]	Shrinkage [%]	Solids content [wt%]	λ [mW/(m · K)]	$E_{horizontal}$ [MPa]	$E_{vertical}$ [MPa]
5WF100	349 ± 3	39.9 ± 0.5	19.9 ± 1.1	102.7 ± 1.3	64.0 ± 20.4	33.4 ± 17.7
10WF100	-	56.2 ± 0.0	19.1 ± 0.1	-	-	-
5WF100GP20	338 ± 5	35.6 ± 1.0	21.3 ± 0.4	95.2 ± 9.3	33.0 ± 9.2	28.6 ± 3.6
5WF100ATH20	394 ± 7	38.6 ± 0.0	21.8 ± 0.2	105.9 ± 5.7	40.6 ± 6.6	33.0 ± 7.0
5WF70W30	306 ± 2	27.6 ± 1.1	18.8 ± 0.4	76.0 ± 1.0	26.5 ± 5.0	23.9 ± 5.1
5WF60W40	285 ± 6	22.9 ± 0.1	18.7 ± 0.4	72.5 ± 3.2	21.5 ± 4.8	12.4 ± 3.3
5WF50W50	271 ± 3	19.2 ± 0.2	18.8 ± 0.5	64.2 ± 2.4	16.4 ± 0.7	8.2 ± 1.5
10WF50W50	301 ± 3	27.7 ± 0.1	18.9 ± 0.0	64.2 ± 0.7	16.2 ± 4.1	8.0 ± 1.9
CNF100	-	89.7	10.6	-	-	-
CNF50W50	-	78.7	8.2	-	-	-

systems undergo excessive shrinkage due to capillary collapse. The incorporation of wool fibers further stabilizes the structure by interrupting network densification.

3.3 Thermal conductivity

The incorporation of waste wool fibers reduced thermal conductivity λ significantly, from 103 mW/(m · K) for 5WF100, to 76, 72.5 and 64.2 mW/(m · K) (5WF70W30, 5WF60W40 and 5WF50W50), as listed in Tab. 1. Literature has shown that washed wool can achieve λ-values as low as 35 mW/(m · K) (Fiore et al., 2020). Despite the increase in density and shrinkage found for 10WF50W50 compared to 5WF50W50, the λ value remained the same, at around 64 mW/(m · K). This indicates that the inherent thermal conductivity of wool dominates

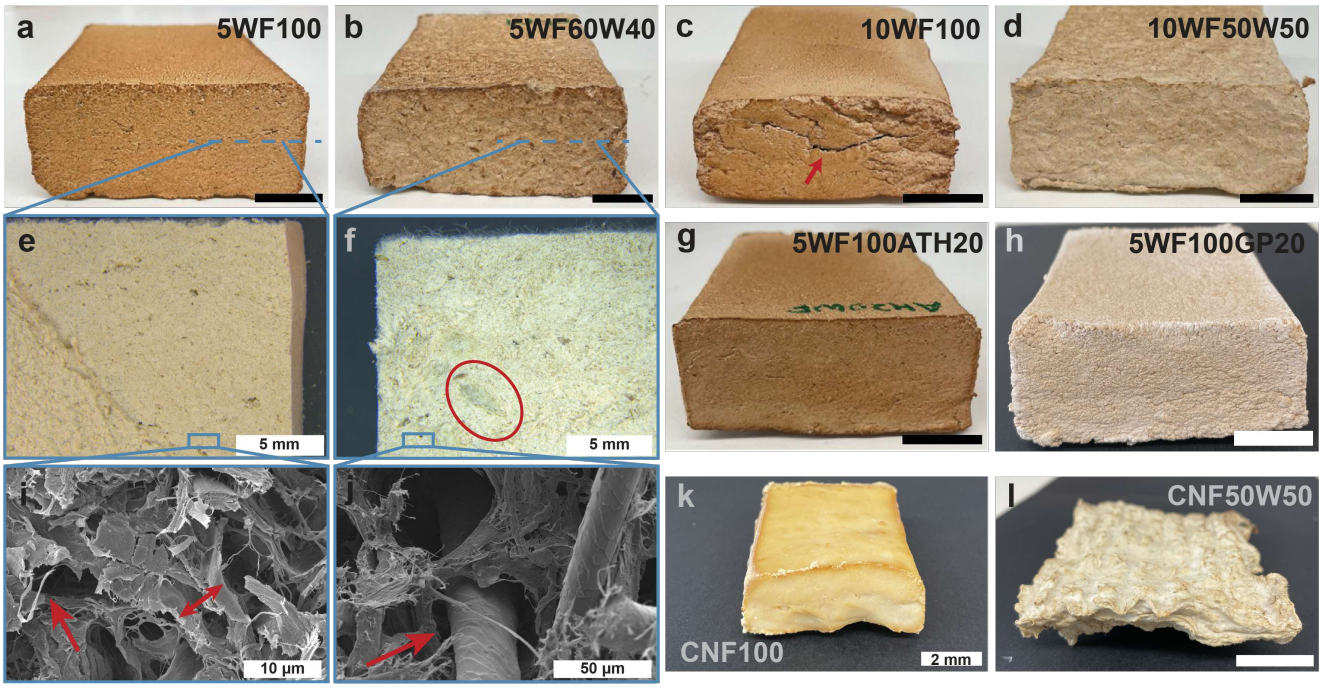


Fig. 4 Finished blocks after molding and drying, scale bars = 2 cm unless otherwise indicated. (a) 5WF100 (b) 5WF60W40 (c) 10WF100, red arrow indicates cracking typical for these blocks (d) 10WF50W50 (e) 5WF100 cross-section, macro-pores are visible (f) 5WF60W40 cross-section, red circle indicates area where wool remained clumped despite mixing. (g) 5WF100ATH20 (h) 5WF100GP20 (i) SEM image of 5WF100, where pores and cavities (red arrows) can be seen alongside WF networks and wood particles (j) SEM image of 5WF70W30: the wool fibers are loosely embedded in the WF matrix, indicated by the red arrow (k) CNF100 (l) CNF50W50

the thermal conductivity behavior of the material as a whole. 5WF100ATH20 and 5WF100GP20 retained a comparable λ-value to that of 5WF100 at 105.9 and 95.2 mW/(m · K), consistent with similar measured densities and shrinkage. The dependence of λ on the density is visualized in Fig. 5f.

By foregoing additional foaming steps, the porosity of the present system was not specifically optimized to achieve the lowest thermal conductivity possible. Further reductions in thermal conductivity could potentially be achieved by tailoring the pore structure, for example through smaller pore sizes and an increased fraction of closed pores (Gibson and Ashby, 1997b). For comparison, Hou et al. (2023) reported a λ value of 48.6 mW/(m · K) for a highly engineered CNF foam produced using sodium dodecyl sulfate (SDS) for foam stabilization and borate cross-linking, resulting in an ultra-low density of 12.1 kg/m^3. By implementing these kinds of strategies on the present WF material, the thermal conductivity and density could be reduced. Within this work, a straightforward manufacturing route was chosen, with the absence of further processing additives, to highlight the potential of combining WF with waste wool fibers to produce thermally insulating materials with reasonable performance using comparatively simple processing and waste-derived feed-stocks.

3.4 Mechanical response and structural anisotropy

The samples under compression exhibited a foam-like response (Fig. 5c): an initial, linear-elastic regime, followed by a plateau, and finally a rapid rise in stress associated with densification (Gibson and Ashby, 1997a). The compression test results are shown in Fig. 5b, where it is shown that the stress response was anisotropic. Samples cut along the horizontal axis had greater Young's moduli E under compression, however the difference could not be related to a formulation specific trend and varied between 11–103 %. The anisotropy itself was linked to compaction from manual molding leading to cell-elongation and in-plane fiber alignment. An additional contribution likely occurred during drying in the convection oven, where density gradients and capillary-driven fiber rearrangement occurred. By introducing a wool fraction, E was reduced. This is linked first to the inherently low stiffness of wool fibers, second to a disruption of WF network connectivity, and third to the loose embedding of the wool fibers in the WF network, as shown in Fig. 4j. Similar reduction in mechanical properties is observed for 5WF100ATH20 and 5WF100GP20, both with a high loading of 20 wt%, disrupting the WF network. Equivalent horizontal (16 MPa) and vertical (8 MPa) E were found for 5WF50W50 and 10WF50W50,

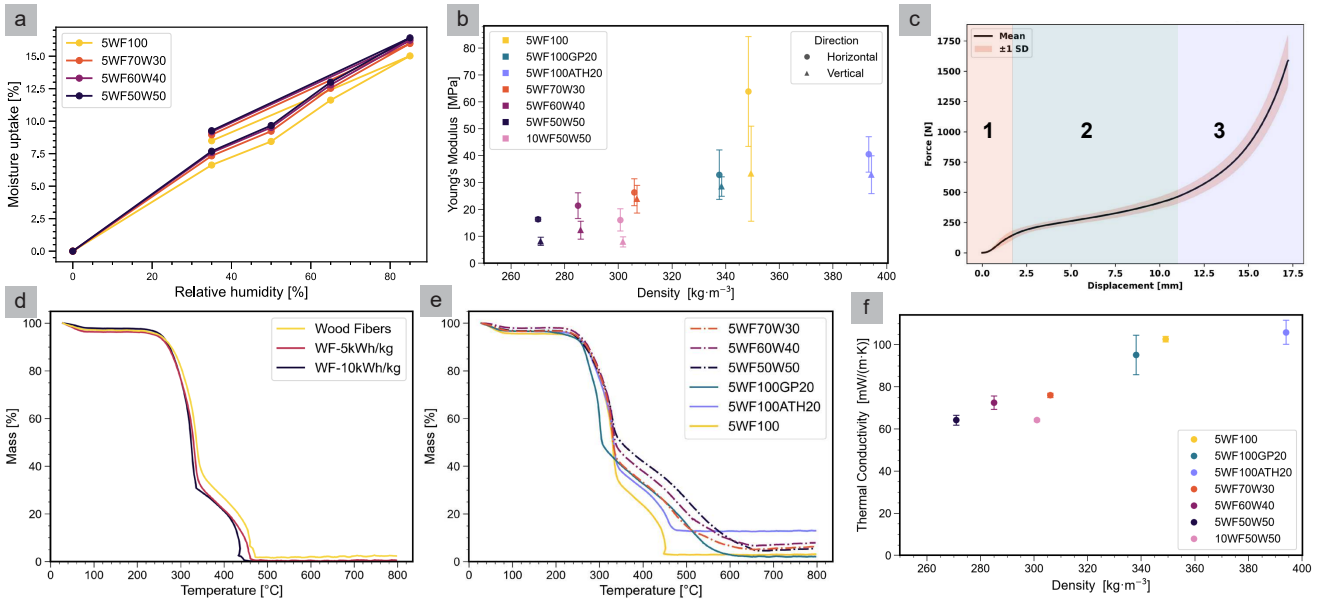


Fig. 5 (a) The plateau values of MU in different relative humidity conditions. By adding wool, the MU can be increased. All samples follow a hysteresis curve upon desorption of moisture. (b) E in compression: there is clear anisotropy derived from molding and drying processes. E is negatively impacted through the addition of wool or a high of flame retardant loading. (c) A typical compression curve showing 1: the elastic region 2: plateau and 3: densification of the foam-like structure (depicted is $5WF60W40_{vertical}$) (d) TGA of wood fibers and WF (5 and 10 kWh/kg_{wood}), where both WF batches exhibited reduced residual mass linked to an increase in surface area. (e) TGA of finished samples: ATH, GP and wool each had a positive effect on slowing the thermal degradation process. (f) λ vs ρ: Samples follow the general trend of greater density leading to an increase in thermal conductivity. Notable here is 10WF50W50, which shows a similar λ-value to 5WF50W50 despite a higher density, indicating a greater influence of the wool fraction on thermal transport properties.

indicating that an increased fraction of WF did not enhance load-bearing capabilities. In fact, when taking the greater density of 10WF50W50 into account, the performance was diminished.

3.5 Thermal stability

An initial comparison of wood fibers, 5WF, and 10WF via TGA under air is shown in Fig. 5d. All mass loss and temperature ranges are given in supplementary information S1. The initial mass loss stage corresponded to the evaporation of moisture (−2.3–−3.8 %). The second stage, the largest, was associated primarily with hemicellulose and cellulose decomposition. This occurred between 300–345 °C and led to mass losses of around −70 %. Subsequent mass loss (25–28 %) was attributed to oxidative degradation of lignin-rich residues (440–492 °C). The inflection in mass loss around 450 °C is attributed to exothermic oxidation reactions interfering with the heating rate. The residual masses were measured as 0, 0.3 and 2.4 % for 5WF, 10WF and wood fibers, respectively. The fibrillated samples exhibited slightly lower degradation onset temperatures and residual masses than that of the wood fibers. This indicates enhanced oxidation of the fibrillated material, due to increased surface area and structural disruption resulting from the fibrillation process. An increased residual mass can additionally be attributed to a higher extractives and ash content in the wood fibers, which are likely to have been washed away after dewatering post-fibrillation.

For the molded and dried samples, TGA results (under air) are displayed in Fig. 5e. 5WF100 blocks, containing no additional flame retardant, exhibited the same degradation behavior as the source material, indicating that the processing method did not influence the primary decomposition stages. The residual mass was found to be 3 %. Samples containing wool (5WF70W30, 5WF60W40, and 5WF50W50) exhibited distinctly slower degradation behavior, correlated to the wool fraction, with a higher wool fraction leading to slower mass loss above 300 °C. The residual masses were 5.2, 7.9 and 5.4 % for 30, 40 and 50 % respectively. Through the addition of GP and ATH, the degradation onset temperature was lowered to 296 and 324 °C respectively. 5WF100ATH20 resulted in a residual mass of approximately 12 %, significantly higher than that of the untreated samples. This is associated with the presence of thermally stable aluminum oxide alongside an increased development of carbonaceous char. 5WF100GP20 exhibited gradual

Table 2 Temperature ranges from preliminary horizontal single-flame tests, over a duration of 2 min. The maximum temperature that could be recorded was 355 °C, thus temperatures may be higher than indicated.

Sample	Early [°C]	1 min [°C]	2 min °[C]
5WF100	294–355+	355+	355+
5WF100ATH20	297	206–252	143–228
5WF100GP20	157–259	51–60	32–39
5WF70W30	355+	133–295	46–294
5WF60W40	318–352	53–57	32–34
5WF50W50	137–265	48–53	31–33

mass losses, connected to early carbonisation, however there is a comparably low residual mass, 2 %, to samples containing ATH. Although GP was transported to the surface, the bulk exhibits distinct thermal degradation behavior when compared to 5WF100.

3.6 Flammability behavior

Selected video frames from the flammability tests are shown in Fig. 6, with the surface temperature development provided in Tab. 2. Samples consisting solely of fibrillated wood (5WF100, Fig. 6a) developed and sustained flames, with the formation of smoke and ash. The surface temperature remained above 350 °C. 5WF100ATH20 (Fig. 6b) continuously produced smoke without visible flaming, connected to the release of water vapor, but had a slow reduction in surface temperature, not falling below 143 °C after two minutes. 5WF100GP20 (Fig. 6c) did not visibly ignite and had a rapid fall in surface temperature to below 40 °C, indicating effective promotion of condensed-phase mechanisms and char formation, despite the inhomogeneous distribution. At 30 wt% wool content, Fig. 6d, inconsistent responses were observed, with some samples sustaining combustion. At 40 and 50 wt% wool, in Fig. 6e/f, consistent self-extinguishing behavior was achieved, accompanied by a rapid surface temperature reduction, ranging between 31–34 °C after two minutes. This trend aligns with the inherent flame resistance of wool, which promotes carbonization over flaming combustion, in addition to producing lower heat and smoke emissions. Different flame retardant strategies were explored in this work. The two additive routes were compatible within a fibrillated wood system, although GP, while the more effective in promoting self-extinguishing behavior, shows issues with water transport during processing and drying. Each system additionally reduced mechanical stiffness due to the necessity for high loading.

3.7 Moisture uptake

The materials displayed hygroscopic properties upon transfer between progressively higher humidity chambers, with all samples exhibiting a gain in MU (Fig. 5a). From the dry state to 35, 50, 65 and 85 % RH, 5WF70W30 had a moisture uptake (MU) of 7.3, 9.2, 12.5 and 16.0 %, 5WF60W40 had 7.6, 9.5, 12.8 and 16.2 % MU, and 5WF50W50 showed an MU of 7.7, 9.7, 13.0 and 16.4 %. The addition of wool increased the MU in comparison to 5WF100, which had an MU of 6.6, 8.4, 11.6 and 15.0 %. This behavior is consistent with the inherently higher moisture adsorption capacity of wool fibers, attributed to its keratin based structure, which contains numerous polar functional groups (Simonič and Zemljič, 2020). When the samples were moved from 85 % RH to 35 % RH, a hysteresis effect was observed, linked to capillary condensed water in cellulosic materials (Fredriksson and Thybring, 2019), and transformation of meta-stable inter-chain bonds during swelling in wool (Downes and Mackay, 1958). 5WF70W30 reduced down to 9.0 % MU, 5WF60W40 to 9.2 % MU, 5WF50W50 to 9.3 % MU, and 5WF100 to 8.5 % MU. Hygroscopic materials have been shown to stabilize indoor humidity through moisture buffering (Yang et al., 2022), associated with a positive effect on personal health and comfort, as well as with durability and energy efficiency of buildings (Zhang et al., 2017a,b).

3.8 Application potential and material positioning

In order to contextualize the porous materials developed in this work within the current market, the following section will explore the application potential through comparison with market-available materials. The materials developed within this work were tested for multiple properties including density, ρ, (271–394 kg/m^3), Young's modulus in compression, E, (8–64 MPa), and thermal conductivity, λ, (64–103 $mW/(m \cdot K)$). Considering these parameters, the resulting porous materials are currently best suited for non-structural applications such as protective packaging. Their moderate thermal insulation performance, together with moisture buffering and ability to be combined with additives such as flame-retardants, also suggests potential for interior insulation products following further structural optimization.

Packaging accounts for the largest share of polymer use at 26 % (MacArthur et al., 2016). One common packaging material is expanded polystyrene (EPS), which has an E of 3.5–80 MPa under compression, and a reported λ-value of 30 $mW/(m \cdot K)$ (Krundaeva et al., 2016; Yoo et al., 2021). Cork, a sustainable alternative, performs at 14–26 MPa, with a λ-value of 45 $mW/(m \cdot K)$ (Anjos

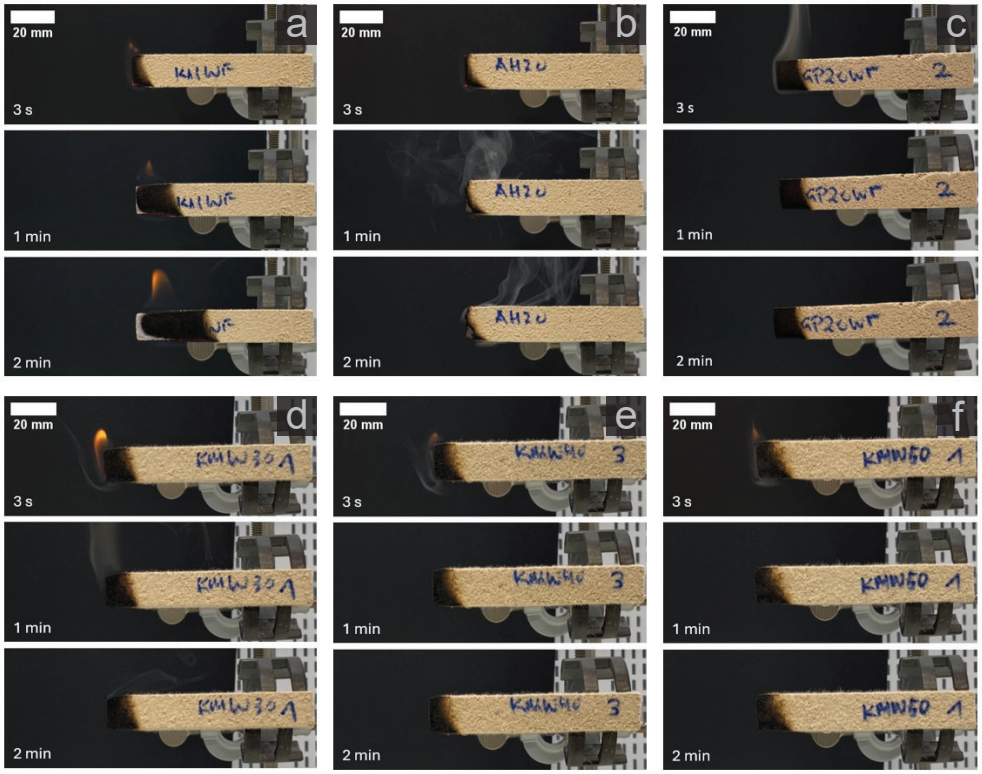


Fig. 6 Selected frames from horizontal single-flame tests. (a) 5WF100, self-sustaining flame with smoke and ash formation (b) 5WF100ATH20, no visible flaming, however smoke or vapor was continuously produced throughout (c) 5WF100GP20, no observed flame (d)-(f) 5WF70W30, 5WF60W40, and 5WF50W50: as wool content increased, so did the reliability of self-extinguishing behavior, where all 40 and 50 % wool samples self-extinguished.

et al., 2014; Matias et al., 1997), see Tab. 3. Both are cellular solids, which follow the same compressive response as observed in this work, characterized by an initial elastic region followed by a plateau, ideal for the type of cushioning behavior needed during transportation. When functioning as packaging material, the transported goods must be protected from thermal fluctuations, making a low thermal conductivity a vital property of packaging materials. Current market-viable cellulose foams, made for acoustic paneling, have had relatively low reported compression moduli of 0.17–0.5 MPa for densities of 82–94 $\mathrm{kg/m^3}$, although no thermal properties were found in relation to this material (Valkonen et al., 2023). In comparison, fibrillated wood composites developed in this work have shown E under compression of 8–64 MPa, however for a higher density. As the weight of a packaging material greatly affects the economic viability, further structural tuning could be necessary for industrial relevance. With λ-values of 64–103 $\mathrm{mW/(m \cdot K)}$, achieved even at these higher densities, it is feasible that the thermal properties could be tuned to an acceptable value for packaging or even insulation materials. In Tab. 3, more materials commonly used in packaging and insulation, as well as some more recent development in the wood and cellulose foam space are listed, in order to show where this work is positioned based on the achieved properties.

Beyond its mechanical and thermal performance, the hybrid materials developed in this work offer additional functionalities that increase their potential for sustainable applications. The incorporation of waste wool reduced drying shrinkage, resulting in improved dimensional stability and higher material yield during processing. Unlike other studies conducted on wool-based insulation, which often rely on synthetic binders such as polyester fibers or acrylic-polyurethane resins (Dénes et al., 2022; Mazhikhanova et al., 2025), structural integrity in the present work is provided solely by WF networks. Eliminating petroleum-based binders improves the renewable content of the material and may additionally simplify end-of-life treatment.

Despite the promising functionality, industrial implementation of the developed materials may require a reduction in density through an improved pore architecture. The waste wool fiber dispersion, as well as more efficient sample drying, could be improved during a scale-up process.

Table 3 List of typical packaging and insulating materials and their properties

Material	Function	Density [kg/m^3]	E [MPa]	λ [mW/(m · K)]	Source
Glass wool	Insulation	60	-	36	(Yoo et al., 2021)
Sheep wool	Insulation	10–20	-	38–54	(Kumar et al., 2020)
EPS foam	Packaging	40–120	3.5–80	30	(Krundaeva et al., 2016; Yoo et al., 2021)
Cork	Packaging	95–210	14–26	45	(Matias et al., 1997; Anjos et al., 2014)
Cellulose foams	Interior	82–94	0.17–0.5	-	(Valkonen et al., 2023)
Cellulose foam (SDS)	Research	12.1	-	48.6	(Hou et al., 2023)
Wood fiber foam	Research	45–200	-	40–80	(Bunzel et al., 2017)
Wood fibril hybrids	Research	271–394	8–64	64–103	This work

4 Conclusion

In this work, porous materials were produced using residual wood that was fibrillated with minimal processing steps. This streamlined approach only necessitated the input of 5 kWh/kg$_{\text{wood}}$ in order to achieve sufficient network connectivity and form-stable blocks. In fact, a higher fibrillation energy of 10 kWh/kg$_{\text{wood}}$ reduced stability during drying, causing cracks. When comparing commercially sourced CNF to the WF produced in this work, the samples reached a shrinkage of 89.7 % (as compared to 73 % at similar solids content of 8 wt%, and 40–56 % at 19 wt%), showing that residual wood particles in the WF dispersion can aid in maintaining form-stability. Mixing and molding were both done through simplified processes, and drying was completed in a convection oven, showing potential for a straightforward scale-up. By using industrial wool waste, λ-values as low as (64.2 ± 2.4) mW/(m · K) were achieved, in addition to a higher material yield. Increased moisture uptake and inherent flame retardancy were introduced into the system through the use of waste wool. The WF network provided stability even when incorporating up to 50 wt% wool, excluding the need for chemical binding agents. It was also shown that wool fibers can be mixed with WF and wood particles to create largely homogeneous materials, although more intensive mixing is needed to reduce fiber clumps. The wool fibers were only loosely embedded in the WF matrix and there was minimal mechanical interaction between the two components, which resulted in the reduction of compressive stiffness. When investigating practical use cases, ATH and GP were successfully incorporated, with GP showing reliable preliminary self-extinguishing properties, but unsatisfactory distribution in the dried material. Thus a simplified and streamlined method was developed for valorizing bio-based waste streams of both wood and wool. Future work should focus on reducing the density of the porous materials, targeting more foam-like structures.

Acknowledgements SEM imaging was performed by Anja Huch (Empa), to whom we are additionally thankful for her technical assistance during this project. We thank Gustav Nyström for supporting this work within the Cellulose and Wood Materials Laboratory, as well as for the helpful input and discussions. The authors also gratefully acknowledge Ingo Burgert (ETH Zürich) for input and master thesis supervision, Samuel Brunner (Empa) for supporting and discussing thermal conductivity measurements, and Roman Elsener (Empa) for supporting the mechanical testing.

Funding

The authors declare that no grants were received during the preparation of this work. Research support was provided by Empa (Cellulose & Wood Materials Laboratory).

Data availability

The data is available from the corresponding author upon reasonable request.

Competing interests

The authors declare no competing interests.

References

Adu S, Adu G, Frimpong-Mensah K, Antwi-Boasiako C, Effah B, Adjei S (2014) Maximizing wood residue utilization and reducing its production rate to combat climate change. International Journal of Plant and Forestry Sciences 1(2):1–12

Anjos O, Rodrigues C, Morais J, et al (2014) Effect of density on the compression behaviour of cork. Materials & Design 53:1089–1096

Antonini C, Wu T, Zimmermann T, Kherbeche A, Thoraval MJ, Nyström G, Geiger T (2019) Ultra-Porous Nanocellulose Foams: A Facile and Scalable

Fabrication Approach. Nanomaterials 9(8):1142, DOI 10.3390/nano9081142

BFS (2026) Tierbestände der Landwirtschaftsbetriebe. https://www.bfs.admin.ch/asset/de/36583176, accessed: 2026-07-27

van den Born G, van Minnen J, Olivier J, Ros J (2014) Integrated analysis of global biomass flows in search of the sustainable potential for bioenergy production

Bunzel F, Ritter N, Scholtyssek J (2017) Holzschaum - eine alternative zu petrochemischen schaumstoffen. Holztechnologie 58:46–51

Camilli F, Focacci M, Dal Prà A, Bortolu S, Ugolini F, Vagnoni E, Duce P (2025) Turning Waste Wool into a Circular Resource: A Review of Eco-Innovative Applications in Agriculture. Agronomy 15(2):446, DOI 10.3390/agronomy15020446

Canto JATD, Malfait WJ, Wernery J (2023) Turning waste into insulation – a new sustainable thermal insulation board based on wheat bran and banana peels. Building and Environment 244:110740

Downes JG, Mackay BH (1958) Sorption kinetics of water vapor in wool fibers. Journal of Polymer Science 28:45–67

Dudnyk Y, Kulha P, Procházka V, Nyström G, Geiger T (2025) Printed circuit board substrates derived from lignocellulose nanofibrils for sustainable electronics applications. Scientific Reports 15(1):8080, DOI 10.1038/s41598-025-91653-1

Dénes TO, Iştoan R, Tâmaş-Gavrea DR, et al (2022) Analysis of sheep wool-based composites for building insulation. Polymers 14:2109

EEA (2026) Material stocks in a circular economy. https://www.eea.europa.eu/en/analysis/publications/material-stocks-in-a-circular-economy, Accessed: 2026-07-27

Fiore V, Bella GD, Valenza A (2020) Effect of sheep wool fibers on thermal insulation and mechanical properties of cement-based composites. Jounral of Natural Fibers 17:1532–1543

Fredriksson M, Thybring EE (2019) On sorption hysteresis in wood: Separating hysteresis in cell wall water and capillary water in the full moisture range. PLoS One 14:e0225111

Gibson LJ, Ashby MF (1997a) The mechanics of foams: basic results, Cambridge University Press, p 175–234. Cambridge Solid State Science Series

Gibson LJ, Ashby MF (1997b) Thermal, electrical and acoustic properties of foams, Cambridge University Press, p 283–308. Cambridge Solid State Science Series

Hou Y, Liao J, Huang L, et al (2023) Plant bio-inspired laminar cellulose-based foam with flame retardant, thermal insulation and excellent mechanical properties. Journal of Materials Chemistry A 11:1138–1147

Josset S, Hansen L, Orsolini P, Griffa M, Kuzior O, Weisse B, Zimmermann T, Geiger T (2017) Microfibrillated cellulose foams obtained by a straightforward freeze–thawing–drying procedure. Cellulose 24(9):3825–3842, DOI 10.1007/s10570-017-1377-8

Krundaeva A, Bruyne GD, Gagliardi F, et al (2016) Dynamic compressive strength and crushing properties of expanded polystyrene foam for different strain rates and different temperatures. Polymer Testing 55:61–68

Kumar D, Alam M, Zou PX, et al (2020) Comparative analysis of building insulation material properties and performance. Renewable and Sustainable Energy Reviews 131:110038

Kunttu J, Hurmekoski E, Heräjärvi H, Hujala T, Leskinen P (2020) Preferable utilisation patterns of wood product industries' by-products in Finland. Forest Policy and Economics 110:101946, DOI 10.1016/j.forpol.2019.101946

Lawrence CA (2003) Fundamentals of spun yarn technology. CRC Press

LID (2025) «Wolle sollte kein Abfallprodukt sein». https://www.lid.ch/artikel/wolle-sollte-kein-abfallprodukt-sein, Accessed: 2026-07-27

MacArthur E, Waughray D, Stuchtey MR (2016) The new plastics economy - rethinking the future of plastics. The World Economic Forum

Mad'in (2025) Europe's Forgotten Wool: History, Waste and the Future of a Sustainable Fibre - Mad'in Europe. https://www.madineurope.eu/en/europes-forgotten-wool/, Accessed: 2026-07-31

Malinverno N, Buschor S, Vogel K, Schwarze F, Stadelmann G, Thürig E, Nowack B, Nyström G, Som C (2024) Resolving complexity: Material flow analysis of a national wood flow system integrating the versatility of wood. Journal of Industrial Ecology 28(6):1716–1729, DOI 10.1111/jiec.13560

Matias L, Santos C, Reis M, et al (1997) Declared value for the thermal conductivity coefficient of insulation corkboard. Wood Science and Technology 31:355–365

Mazhikhanova B, Shardarbek M, Junisbekov M, et al (2025) Application of raw sheep wool waste for the production of sustainable and energy-efficient insulation materials. Textile Research Journal 0:00405175251380818

Miao X, Hua W, Li Y, Bian F, Xiao T (2024) Extraction of cellulose nanofibrils from pine sawdust by integrated chemical pretreatment. Heliyon 10(3):e25355, DOI 10.1016/j.heliyon.2024.e25355

Sahateollisuuskirja (2026) Sawmills' by-products as a raw material. https://sahateollisuuskirja.fi/en/puuraaka-aine/sahateollisuuden-sivutuotteet-raaka-aineena/,

accessed: 2026-07-27

Simonič M, Zemljič LF (2020) Functionalized wool as an efficient and sustainable adsorbent for removal of zn(ii) from an aqueous solution. Materials 13:3208

Sjöström E (1993) Wood chemistry: fundamentals and applications, second edition edn. Academic Press, San Diego

Solala I, Iglesias MC, Peresin MS (2020) On the potential of lignin-containing cellulose nanofibrils (LCNFs): a review on properties and applications. Cellulose 27(4):1853–1877, DOI 10.1007/s10570-019-02899-8

SRF (2019) Mal Nutztier, mal Schädling - Die Geschichte vom guten und vom bösen Schaf. https://www.srf.ch/news/schweiz/mal-nutztier-mal-schaedling-die-geschichte-vom-guten-und-vom-boesen-schaf, Accessed: 2026-07-27

SRF (2022) Schafwolle aus der Schweiz - Vom Abfallprodukt zum vielseitig nutzbaren Rohstoff. https://www.srf.ch/news/schafwolle-aus-der-schweiz-vom-abfallprodukt-zum-vielseitig-nutzbaren-rohstoff, Accessed: 2026-07-27

SRF (2025) Schweizer Schafwolle muss tonnenweise entsorgt werden. https://www.srf.ch/news/schweiz/kein-platz-mehr-schweizer-schafwolle-muss-tonnenweise-entsorgt-werden, Accessed: 2026-07-27

Tarrés Q, Oliver-Ortega H, Boufi S, Àngels Pèlach M, Delgado-Aguilar M, Mutjé P (2020) Evaluation of the fibrillation method on lignocellulosic nanofibers production from eucalyptus sawdust: A comparative study between high-pressure homogenization and grinding. International Journal of Biological Macromolecules 145:1199–1207, DOI 10.1016/j.ijbiomac.2019.10.046

Thomas B, Fishwick M, Joyce J, van Santen A (2012) A Waste Footprint Assessment for UK Clothing. Tech. Rep. RNF100-009, WRAP

Valkonen MJ, Cucharero J, Lokki T, et al (2023) Preparation of fully bio-based sound absorbers from waste wood and pulp fibers by foam forming. BioResources 18:2657–2669

Wang QQ, Zhu JY, Gleisner R, Kuster TA, Baxa U, McNeil SE (2012) Morphological development of cellulose fibrils of a bleached eucalyptus pulp by mechanical fibrillation. Cellulose 19(5):1631–1643, DOI 10.1007/s10570-012-9745-x

Weldesemayat Sileshi G, Barrios E, Lehmann J, Tubiello FN (2025) An organic matter database (OMD): consolidating global residue data from agriculture, fisheries, forestry and related industries. Earth System Science Data 17(2):369–391, DOI 10.5194/essd-17-369-2025

Wemmer J, Gossweiler E, Fischer P, Windhab EJ (2019) Effect of foaming on mechanical properties of microfibrillated cellulose-based porous solids. Cellulose 26(4):2487–2497, DOI 10.1007/s10570-018-02228-5

Yang M, Kong F, He X (2022) Moisture buffering effect of hygroscopic materials under wall moisture transfer. Indoor and Built Environment 31:80–95

Yoo J, Chang SJ, Yang S, et al (2021) Performance of the hygrothermal behavior of the clt wall using different types of insulation; xps, pf board and glass wool. Case Studies in Thermal Engineering 24:100846

Yousefi H, Azari V, Khazaeian A (2018) Direct mechanical production of wood nanofibers from raw wood microparticles with no chemical treatment. Industrial Crops and Products 115:26–31, DOI 10.1016/j.indcrop.2018.02.020

Zhang H, Yoshino H, Hasegawa K (2017a) Practical moisture buffering effect of three hygroscopic materials in real-world conditions. Energy and Buildings 139:214–223

Zhang M, Qin M, Rode C, Chen Z (2017b) Moisture buffering phenomenon and its impact on building energy consumption. Applied Thermal Engineering 124:337–345

Zhang Q, Ma L, Zhang X, Zhang L, Wang Z (2022) Lignocellulose nanofiber/polylactic acid (LCNF/PLA) composite with internal lignin for enhanced performance as 3D printable filament. Industrial Crops and Products 178:114590, DOI 10.1016/j.indcrop.2022.114590

Ämmälä A, Sirviö JA, Liimatainen H (2021) Energy consumption, physical properties and reinforcing ability of microfibrillated cellulose with high lignin content made from non-delignified spruce and pine sawdust. Industrial Crops and Products 170:113738, DOI 10.1016/j.indcrop.2021.113738

Supplementary Files

This is a list of supplementary files associated with this preprint. Click to download.

- SupplementaryInformation.docx